PCCP

ROYAL SOCIETY OF CHEMISTRY

PAPER

View Article Online
View Journal | View Issue

Cite this: *Phys. Chem. Chem. Phys.*, 2024, **26**, 14651

Theoretical insight into H_2O impact on V_2O_5/TiO_2 catalysts for selective catalytic reduction of NO_x†

Boyu Wu, Shengen Zhang,* Mingtian Huang, Shengyang Zhang, Bo Liu and Bolin Zhang*

H_2O in flue gas causes the deactivation of V_2O_5/TiO_2 catalysts for selective catalytic reduction (SCR) of NO_x with NH_3 at low temperatures. Developing water resistance requires understanding the theoretical mechanism of H_2O impact on the catalysts. The aim of this work was to clarify the adsorption process of H_2O and the deactivation mechanism induced by H_2O through density functional theory (DFT). The process of H_2O adsorption was studied based on a modeled V_2O_5/TiO_2 catalyst surface. It was found that H_2O had a strong interaction with exposed titanium atoms. Water adsorption on the catalyst surface significantly alters the electronic structure of VO_x sites, transforming Lewis acid sites into Brønsted acid sites. Exposed titanium sites contribute to the decrease of Lewis acidity *via* adsorbed water. *Ab initio* thermodynamic calculations show that H_2O adsorption on V_2O_5/TiO_2 is stable at low coverage but less favorable at high coverage. Adsorption of NH_3 is the most critical step for the SCR of NO_x, and the adsorption of H_2O can hinder this process. The H_2O coverage below 15% of adsorption sites could enhance the NH_3 adsorption rate and have a limited effect on the acidity, while higher coverage impeded the adsorption ability of VO_x sites. This work provided electron-scale insight into the adsorption impact of H_2O on the surface of V_2O_5/TiO_2 catalysts, presented thermodynamic analysis of the adsorption of H_2O and NH_3, paving the way for the exploration of V_2O_5/TiO_2 catalysts with improved water resistance.

Received 29th February 2024,
Accepted 18th April 2024

DOI: 10.1039/d4cp00893f

rsc.li/pccp

1. Introduction

Nitrogen oxides (NO_x) are major atmospheric pollutants that lead to significant environmental issues including acid rain, smog, global warming and depletion of the ozone layer.[1–4] Over the last four decades, substantial research has been invested in addressing the NO_x dilemma. Among the various NO_x reduction technologies developed, the V_2O_5/TiO_2 selective catalytic reduction (SCR) catalyst has become particularly notable.[5,6] It has been widely implemented to control NO_x emissions from diverse sources, such as coal-fired power plants, sintering plants, vehicles, and multiple industrial operations. The commercial vanadium-based catalysts can achieve excellent NO_x removal across a broad temperature spectrum (150–450 °C), and provide better resistance towards poisoning factors than other catalysts.[7–9]

The impact of water vapor on the performance of low-temperature SCR systems presents a complex picture. Numerous studies have consistently shown that water vapor significantly reduces the NO_x removal rate of SCR catalysts at low temperatures, 5% of water vapor in the gas stream can cause 10–20% percent of decrease of NO_x conversion rate at low temperatures (150–200 °C).[9,10] There has been an active effort to develop catalysts more resistant towards water, however these studies primarily focus on the reactivity and active species involved.[11] An understanding of the effect of water molecules on the surface is lacking, despite water being commonly present in industrial exhausts.

The consensus attributes this decrease to water molecules interfering with the adsorption of reactants or their subsequent reactions on the catalyst surface, thereby decreasing NO_x removal rate.[12–14] Qing *et al.*[14] found that the presence of H_2O inhibited NH_3 adsorption, resulting in a significant decrease in NO conversion. However, Inomata *et al.*[15] suggests water vapor may also facilitate the formation of additional Brønsted acid sites on certain vanadium-based catalysts, thus improving the low temperature activity. Additionally, water has a lower adsorption energy than NH_3 on vanadium oxide surfaces. This discrepancy highlights critical gaps in understanding the intricate interactions between water vapor and catalytic surfaces at low-temperature, and how it can affect the catalytic performance.

Numerous studies have explored the configuration of vanadium species on surfaces. The calcination temperature for an SCR catalyst typically falls within the range of 300–600 °C.[16]

Institute for Advanced Materials and Technology, University of Science and Technology Beijing, Beijing 100083, China.
E-mail: zhangshengen@mater.ustb.edu.cn, zhangbolin@ustb.edu.cn

† Electronic supplementary information (ESI) available. See DOI: https://doi.org/10.1039/d4cp00893f

Within this range, V_2O_5 tends to develop a crystalline film on the support structure. However, this temperature is not sufficiently high to facilitate the formation of V_2O_5 ''towers'' – vertically oriented crystal structures.[17,18] This observation has been confirmed through X-ray adsorption spectroscopy.[19–21] Catalayud *et al.*[22] suggest that on the TiO_2 anatase (001) surface, the most stable arrangement for V_2O_5 is linear, lying in the [010] direction. Wilcox *et al.*[23] proposed a sub monolayer configuration to represent a low loading (<2 wt%) vanadium surface with free surface titanium atoms exposed. This model, by intentionally exposing free surface titanium atoms, enabled the investigation of water's molecular interactions with the catalyst surface and the subsequent effects on mercury oxidation. Importantly, this configuration explicitly considered the significant interaction between TiO_2 and water molecules, a critical factor at low vanadium loadings. Lian *et al.*[24] suggest that a V_2O_5 loading of 4 to 8 wt% achieves satisfactory low-temperature NO_x reduction rates. Yet, at higher loadings, experimental results indicate that the TiO_2 surface becomes less exposed,[18,25] leading to fewer free titanium atoms available to interact with water molecules. Saleh *et al.*[18] observed a high V/Ti ratio on the surface of a low-temperature SCR catalyst, as suggested by XPS and XANES results. They found that at high vanadium loadings (7 wt%) on anatase surfaces, polymeric vanadium stripes almost completely cover the anatase (001) surface.

The (001) surface of anatase TiO_2 is widely employed in commercial SCR catalysts as a support for active species, and the (001) surface has been chosen for most of the theoretical works. The anatase surface has a high surface area and strong metal–support interaction,[16,26,27] attracting active species to enhance catalytic activity and stability.[26,28–30] Furthermore, it has a well-defined structure and rich surface chemistry, facilitating theoretical modeling and analysis of reaction mechanisms.

The leading theories for the SCR reaction pathway include the Eley–Rideal mechanism, characterized by the reaction of adsorbed ammonia with gaseous NO molecules, and the Langmuir–Hinshelwood mechanism, which involves interaction between adsorbed ammonia and adsorbed NO species.[31–33] Regardless of the reaction pathway NH_3 adsorption is an initial and crucial step in the SCR reaction, and in particular its adsorption rate on the Lewis site is the most significant to the catalytic reaction cycle.[14,33,34] In this study, we evaluate the adsorption process and the thermodynamic stability of models with varying levels of water coverage. The influence of the TiO_2 (001) surface and active species during the water adsorption process is explored through DFT calculations and *ab initio* thermodynamic analyses. Models featuring different degrees of water coverage on the V_2O_5/TiO_2 surface were developed to assess their impact on catalytic reactivity and stability. The adsorption behavior of NH_3 derived from these computational results were compared with results from existing experimental and theoretical works. Several paths to enhance the resistance toward water induced deactivation are proposed.

2. Computational methodology

2.1. DFT calculations and modeling

The calculations were performed using the CP2K package (2023.2).[35] We used the mixed Gaussian and plane wave approach to DFT, together with the revised Perdew–Burke–Ernzerhof (revPBE) functional parameters.[36,37] Geometry optimization and vibrational analysis was performed at the triple-ζ basis level (pob-TZVP-rev2);[38] for adsorption position finding, double-ζ basis sets (pob-DZVP-rev2)[38] have been used. An energy cutoff of 400 Ry has been used; the convergence criterion for geometry optimization was set to 1.0×10^{-7}. The semi-empirical dispersion corrections for the van der Waals interactions were applied by employing the Grimme's approach (so called DFT-D3) with Becke and Johnson (BJ) damping.[39,40] To eliminate convergence problems, Fermi–Dirac smearing was employed.

For the stability of the supported systems, V_2O_5 and TiO_2 in bulk form were fully optimized. A 3-layer anatase TiO_2 (001) surface was constructed as the support. To mitigate any potential dipole moments, a vacuum space of 20 Å was introduced along the *Z*-axis. It is widely accepted that three layers of TiO_2 support can adequately represent the support structure.[23,41–44] The *K*-points were selected based on a Monkhorst–Pack grid of $2 \times 7 \times 1$ in real space. For modeling the supported catalyst surface, vanadium species were placed atop the supporting TiO_2, and the model of the supported system was subsequently optimized. The adsorption was studied with extended supercell (15.13×15.13 Å^2). Multiwfn (Version 3.8, release date: 2023-Dec-1) was used to aid input generation and postprocessing of the results.[45]

Water and NH_3 molecules were relaxed separately as isolated molecules in a $30 \times 30 \times 30$ Å^3 periodic cell. The calculated bond lengths for the O–H bond in the H_2O molecule and the N–H bond in the NH_3 molecule are 0.97 Å and 1.02 Å, respectively. These values demonstrate excellent agreement with the corresponding experimental measurements, which are 0.96 Å for H_2O[46] and 1.01 Å for NH_3.[47] The slight difference in bond length might be attributed to the revPBE functional and tends to overestimate the bond length.[48]

2.2. *Ab initio* thermodynamic calculations

DFT calculations have limitations, particularly in simulating real-world conditions. A key limitation is that these calculations do not account for temperature and pressure effects. Consequently, the physical quantities evaluated through DFT are strictly valid only at absolute zero temperature and no pressure. To actually describe the effect of water adsorption at finite temperatures and pressures, DFT calculations should be combined with thermodynamic considerations, and we took a similar path described in previous literature to calculate the Gibbs free energy of adsorption.[23,49–53] The stability of various configurations can be described by the Gibbs free energy of adsorption, at a temperature T and pressure p. The Gibbs free energy terms are defined as $G(T,p) = E_{tot} + F_{vib} - TS^{conf} + pV$. The first term is the total energy E_{tot}, which is directly obtained from the DFT calculations; F_{vib} accounts for the vibrational contributions, and TS^{conf} includes configurational entropy.

As discussed by Cheng *et al.*[52] and Rogal *et al.*,[50] when calculating corrected Gibbs free energy of adsorption, the vibrational contribution of the substrate surface can be neglected given the substrate surface is not being reconstructed in a significant way. Furthermore, the vibrational contribution of the metal oxide surface remains fairly constant at application temperatures for low temperature NO_x removal.[54] However, the vibrational contribution of adsorbates is not neglectable.[23,52,55] According to the harmonic approximation, the vibrational contribution to Gibbs free energy is defined as a frequency and temperature dependent function in eqn (1), where ω_i is the frequency of adsorbate, $\hbar$ is the reduced Planck constant, and k_B is the Boltzmann constant.

$$F^{\text{vib}}(T,\omega) = \sum \frac{1}{2}\hbar\omega_i + k_B T \ln\left(1 - e^{-\hbar\omega_i/k_B T}\right) \quad (1)$$

Gibbs free energy of adsorption $\Delta G(T,p)$ is defined as in eqn (2), where A is the surface area, E_{system} is the Gibbs free energy of the surface with adsorbates, E_{clean} is the free energy of the surface, N_i is the quantity of corresponding adsorbate, and $\mu_i(T,p_i)$ is the chemical potential of the corresponding adsorbate at a given T and p_i.

$$\Delta G(T,p) = \frac{1}{A}\left[E_{\text{system}} - E_{\text{surface}} + \Delta F^{\text{vib}} - \sum N_i \mu_i(T,p_i)\right] \quad (2)$$

The chemical potential: $\mu_i(T,p_i)$ in eqn (2) is defined as eqn (3), where E_i is the total energy produced by DFT calculation; E_i^{ZPE} is the zero point vibrational energy, given there are no vibration-rotation interactions in the adsorption model, E_i^{ZPE} is approximated as $\frac{\hbar}{2}\sum\omega_i$; $\mu_i(T,p_0)$ is defined as $\mu_i(T,p_0) = H - T \times S$, where H represents the enthalpy, S represents the entropy, and values of H and S are freely available from the "NIST-*JANAF* Thermochemical Tables",[56] a copy of the values used in this study is attached in the ESI,† Table S1.

$$\mu_i(T,p_i) = E_i + E_i^{\text{ZPE}} + \mu_i(T,p_0) + k_B T \ln\left(\frac{p_i}{p_0}\right) \quad (3)$$

To investigate the influence of H_2O on the reaction rate, we focused on NH_3 adsorption at the Lewis acid site, a critical step in the SCR reaction mechanism. To further elucidate this, we employed transition state theory and proposed a rate constant in the Arrhenius form: R^{Ads}, as described as eqn (4), where R is the molar gas constant.

$$R^{\text{Ads}} = A \times e^{\frac{-A\times\Delta G(T,p)}{RT}} \quad (4)$$

3. Results and discussion

3.1. Modeling of the sub-monolayer and monolayer V_2O_5 surface on a TiO_2 support

A stable model with appropriate representation of reality is essential for studying water's influence on the catalyst surface. For the high loading supported V_2O_5/TiO_2 system, the vanadium species was modeled with similar geometry as the anatase TiO_2 (001) surface, and two layers of TiO_2 support are allowed to relax, as described in the work of Calatayud *et al.*[22] and Wilcox *et al.*[23] The vanadium species in the sub-monolayer module are characterized by 4-fold coordination, including two adjacent exposed vanadium sites. These species form a linear crystalline structure on the surface, which is separated on the TiO_2 surface to achieve approximately 7–8 VO_x per nm^2 coverage as observed by Raman spectroscopy.[57] This model features three structurally distinct oxygen sites: O(1), the single coordinated terminal oxygen (V═O); O(2), the bridging oxygen (V–O–V); and O(3), the anchoring oxygen (V–O–Ti) is coordinated with three atoms: two vanadium and one titanium atom. Representation of the sub-monolayer is shown in Fig. 1(a) and (b).

A monolayer surface model for extreme high vanadium loading is modeled. It is reported that vanadium tends to form a thin film rather than a vertical growing crystalline structure on the anatase surface.[17,19,57,58] The monolayer model was modeled with a similar approach as our sub-monolayer model, and the uninhabited TiO_2 surface is all covered by V_2O_5 species in this configuration. There is no exposed titanium atom on the (001) surface. This model is compared with existing works and the contribution of TiO_2 substrate during water adsorption is studied. To be noted, this model is widely used in other theocratical works, but the surface coverage of VO_x exceeded the experimental observations.[57,59]

The bond distances of the supported dimers were compared with those from previous experimental and DFT studies. Despite the use of different methodologies, there is a reasonable agreement regarding the bond distances, as summarized in Table 1.

To verify the stability of the model, the formation energy was evaluated. This calculation followed similar steps to those outlined by Wilcox *et al.*, Vittadini *et al.* and Gu *et al.*,[41,62,63] and the formation energy was proposed as a key factor to understand the energy changes occurring during the surface formation process, particularly focusing on the energy variation associated with the inhabiting process of vanadium species.

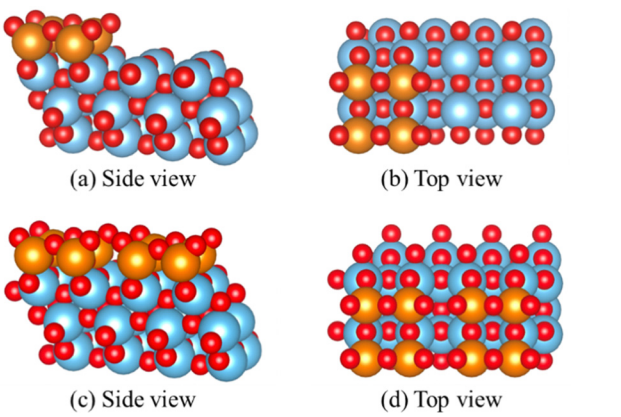

Fig. 1 (a) Side view of the sub-monolayer model; (b) top view of sub-monolayer model; (c) side view of monolayer model; (d) top view of monolayer model. Red are oxygen atoms, blue are titanium atoms, and orange are vanadium atoms.

Table 1 Comparison of calculated bond length and other works

Model	V═O (Å)	V–O bridge (Å)	V–O anchor (Å)
Sub-monolayer (this work)	1.59	1.797	1.94
monolayer (this work)	1.58	1.77	1.94
α-V_2O_5 (experimental)[60]	1.61	1.80	—
V_2O_5 (experimental)[59]	1.58	1.80	—
V_2O_5 (experimental)[61]	1.56	—	—
V_2O_5 layer/TiO_2 (DFT)[62]	1.58	1.78	1.76
V_2O_5 polymeric (DFT)[22]	1.62	1.80	—
V_2O_5 polymeric/TiO_2 (DFT)[22]	1.59	1.82	—
V_2O_5 dimer/TiO_2 (DFT)[27]	1.60	1.80	1.76
V_2O_5 layer/TiO_2 (DFT)[41]	1.60	1.77	1.95

The energy of TiO_2 surface reconstruction is denoted as E_{recon}, using the V_2O_5 bulk phase as a reference, $E_{nVO_{2.5}}$.

The formation energy E_{form} is defined in eqn (5):

$$E_{form} = E_{system} - [E_{nVO_{2.5}} + E_{TiO_2} + E_{recon}] \quad (5)$$

The formation energy for the sub-monolayer model is calculated to be −1.84 eV, indicating strong and stable interaction between the TiO_2 surface and vanadium species in this configuration. The formation energy for the monolayer model is calculated to be −1.23 eV. It is a stable surface structure but compared to the sub-monolayer model it is weaker.

The vibrational frequency was calculated and compared with experimental results. As noted in the literature, the V═O bond exhibits a distinct frequency, typically ranging from 1020 cm^{-1} to 1030 cm^{-1}, attributed to the stretching frequency of this bond.[59,64,65] For both the sub-monolayer and monolayer systems, we calculated the stretching frequency of the V═O bond. In the sub-monolayer model, this frequency corresponds to 1020 cm^{-1}, whereas in the monolayer model, it is observed at 1093 cm^{-1}. A similar increased frequency of the V═O bond was reported by Wilcox *et al.*,[23] who observed an increased frequency of the V═O bond at 1091 cm^{-1} in their model, closely aligning with our results. Our hypothesis is that excessive vanadium loading on the surface reduces the electron negativity of terminal oxygen atoms, resulting in a minor decrease in V═O bond strength. Consequently, this slightly weakened bond requires less energy to vibrate, leading to an increase in the calculated vibrational frequency.

3.2. Water adsorption process

The volume of water is usually around 10 vol% in the fuel gas, applying the ideal gas law in conjunction with Dalton's Law of partial pressures, and the number of water molecules in a finite region can be estimated through eqn (6), where nH_2O is the number of water molecules in the simulation box, P is the atmospheric pressure, V is the volume of the simulation box (15.13 × 15.13 × 30 $Å^3$), R is the ideal gas constant, T is temperature and N_A is Avogadro's number.

$$n_{H_2O} = \frac{10\% \times P \times V}{RT} \times N_A \quad (6)$$

We estimated the quantity of potentially interacting water molecules at temperatures of 300 K, 400 K, and 500 K. The estimated numbers of water molecules in the simulation box are 1.65 × 10^{-3}, 1.24 × 10^{-3}, and 0.99 × 10^{-3}, respectively. As indicated by the relatively small quantity, the deactivation process induced by water is gradual. Thus, for a more accurate representation of reality, H_2O molecules were introduced to the surface sequentially.

The initial position of each H_2O molecule was determined by a surface scanning, which used a mesh grid (30 × 30) located 3 Å above the surface, to identify the most likely locations for H_2O molecule adsorption. After each scan, a water molecule was added to the identified position for adsorption. Once the energy of the system was minimized, this new configuration served as the base for the next scan. The H_2O molecule is always added at the position with the overall highest adsorption energy, thereby avoiding adsorption at positions of local minima.

The scan results for the initial water molecule suggest a preference of adsorption at the interface between V_2O_5 and TiO_2, as evidenced by the higher adsorption energy illustrated in Fig. 2(a). Additionally, the forces acting on the water molecules predominantly point towards the exposed TiO_2 area.

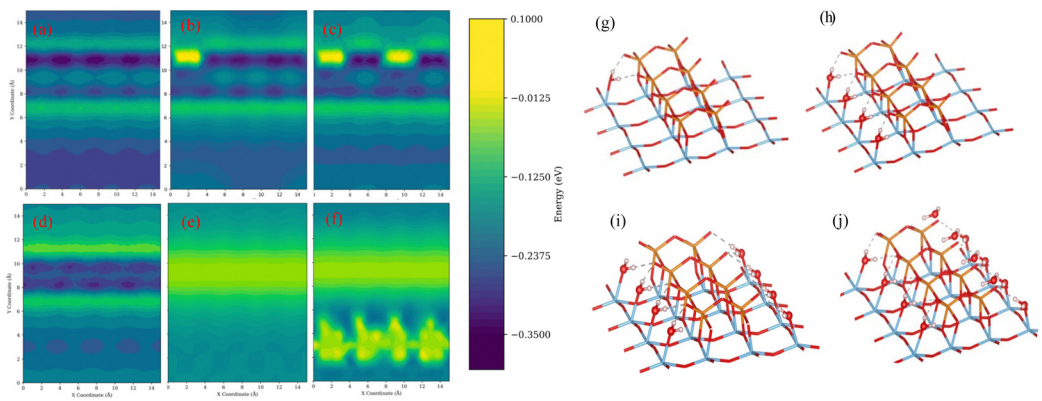

Fig. 2 (a) to (f): The adsorption energy corresponding to models from iterations 0, 1, 2, 4, 8, and 12 (denote sub, sub-1-H_2O, sub-2-H_2O, sub-4-H_2O, sub-8-H_2O, and sub-12-H_2O); (g) to (j): The adsorbed configurations corresponding to models from iterations 1, 4, 8, and 12; Red are oxygen atoms, blue are titanium atoms, orange are vanadium atoms, and light pink are hydrogen atoms; For clarity, 2 layers of TiO_2 support are hidden and the vanadium polymeric stripe is centered.

Considering the insights from the adsorption process calculations, the potential sites for water adsorption on the surface are limited. Each exposed titanium atom is capable of adsorbing one water molecule, and each V_2O_5 species can adsorb one water molecule as well. The surface coverage of water is defined as the ratio of adsorbed water molecules to the maximum adsorption capacity. In this simulation, the maximum capacity for water molecules is determined to be 12.

To have a clearer understanding of the adsorption process, we choose the representative adsorption configurations from the adsorption scan iterations 0, 1, 2, 4, 8, and 12 (denoted as sub, sub-1-H_2O, sub-2-H_2O, sub-4-H_2O, sub-8-H_2O, sub-12-H_2O) for further study, and the corresponding adsorption energy and geometries are illustrated in Fig. 2. It was found that exposed titanium atoms have a strong interaction with the oxygen atoms in water molecules, and the hydrogens are attracted to the terminal oxygen atoms of vanadium species. After the adsorption of the first water molecule, the results from the second scan suggest a noticeable decrease in the adsorption energy around it, as shown in Fig. 2(b), and the corresponding geometry is shown in Fig. 2(g). Due to the repulsion between the terminal oxygen of vanadium species and the oxygen atoms in water molecules, water molecules have shown a preference towards the TiO_2 area due to the repulsion between the terminal oxygen of vanadium species and oxygen atoms in water molecules. Fig. 2(d) and (i) illustrate the corresponding adsorption energy and a model in which 4 water molecules are adsorbed. All four water molecules are in similar configurations after geometry optimization: the oxygen atom in water is bonded with one undercoordinated titanium atom, and the hydrogens of water molecules are attracted to the terminal oxygen of vanadium dimer. The adsorption energy on the exposed TiO_2 area is larger until it is fully covered by water molecules, as illustrated in Fig. 2(e) and (j). Compared to the clean surface, the overall average adsorption energy decreased compared to the clean surface. Subsequent adsorptions occur at the vanadium sites, as shown in Fig. 2(f) and (k). The interaction between the vanadium atom and the oxygen atom in water is not as strong as with titanium. The hydrogen bond between the terminal oxygen and the bridging oxygen of vanadium species contributes most significantly to the adsorption.

To further confirm the interaction between H_2O molecule and TiO_2, a molecular dynamic calculation was carried out at 373 K for 4000 fs with a timestep of 1 fs, using sub-1-H_2O, sub-2-H_2O, sub-4-H_2O, and sub-8-H_2O models. Dissociation of water molecules is evident in the sub-1-H_2O and sub-2-H_2O models, whereas the surface of sub-4-H_2O and sub-8-H_2O models maintains its stability, as illustrated in Fig. 3. The observation of water molecule dissociation and surface reconstruction occurring at lower water coverage levels align with the findings in existing works.[22,23,62,66] The H_2O molecule initially absorbs on the exposed titanium atom, with both H atoms interacting with neighboring terminal atoms from V_2O_5; The Ti–O bond is stretched leading to the formation of 2 Ti–OH groups as shown in Fig. 3(a) and (b). A comprehensive illustration of the dissociation behavior of H_2O is presented in the ESI,† Fig. S1.

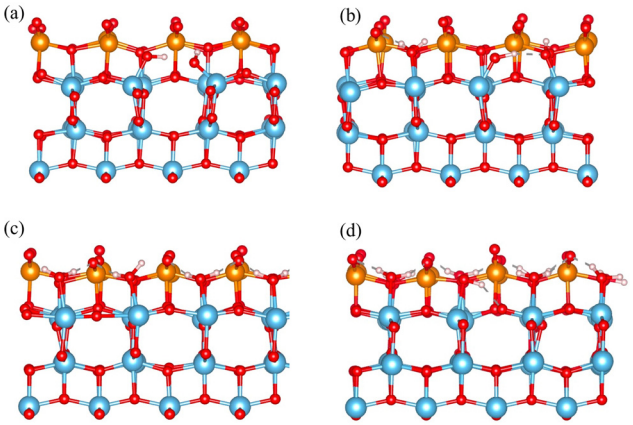

Fig. 3 Molecule dynamic simulation of model sub-1-H_2O, sub-2-H_2O, sub-4-H_2O and sub-8-H_2O at 373 K for 4000 fs. (a)–(d) Side view of sub-1-H_2O, sub-2-H_2O, sub-4-H_2O and sub-8-H_2O after molecule dynamic simulation; red are oxygen atoms, blue are titanium atoms, orange are vanadium atoms, light pink are hydrogen atoms.

Subsequent vibrational calculations for model sub-8-H_2O were also carried out to verify the stability, and the frequencies assignable to the TiO_2 anatase surface were 198 cm^{-1}, 392 cm^{-1}, 579 cm^{-1}, 582 cm^{-1} and 661 cm^{-1}. These peaks are slightly shifted but indicate a stable surface, as experimentally observed by Ohsaka *et al.*[67]

The difference in the interaction of water and the modeled V_2O_5/TiO_2 surface observed in this study and existing works might be due to the slightly different vanadium model and different approaches. The model used in this study is more stable as indicated by the formation energy comparison and vibrational analysis. Also, the lateral influence and angle of water molecule can greatly affect the adsorption process as shown in Fig. 2(a) to (d), and the yellow stripe at $y = 7$ and $y = 12$ can be attributed to the lateral interaction between water molecules and vanadium sites.

The adsorption behavior of water suggests that the presence of exposed titanium atoms enhances water adsorption, with the interface between V_2O_5 and TiO_2 acting as a reservoir for water molecules. Molecular dynamics calculations at 373 K confirm that at a low level of water coverage (one water molecule per surface), water molecules are dissociated upon adsorption; at higher levels of water coverage, the TiO_2 support maintains its stability.

3.3. Electronic structure changes

3.3.1. Projected density of states (PDOS). We observed a notable increase in the Fermi levels, as illustrated in Fig. 4. Projected density of states of models with different water coverage levels are shown. Black arrows indicate the shift of peaks. For configurations with 1, 2, 4, and 8 water molecules adsorbed, the Fermi level shift is proportional to the square of the number of water molecules adsorbed. This upward trend is consistent with Wolkenstein's adsorption theory.[68] However, it is important to note that Wolkenstein's theory does not account for dispersion forces and the potential formation of hydrogen

bonds, which could enhance the adsorption rate of NH_3. Beyond the adsorption of 8 water molecules, the Fermi level shift becomes marginal, suggesting the saturation of water adsorption capacity. Higher Fermi levels can indicate the occupation of free orbitals that can assist adsorption in the adsorbate, thereby reducing electron transfer and potentially weakening the adsorption of both H_2O and NH_3.

The PDOS for the terminal oxygen atoms and vanadium atoms were analyzed, as depicted in Fig. 4. For configurations involving 1, 2, 4, and 8 water molecules adsorbed, a pronounced shift in the PDOS peaks is observed for both the oxygen atoms and the p orbitals of the vanadium atoms. However, this shift becomes less noticeable when the number of adsorbed water molecules increases from 8 to 12. This observation indicates that during the adsorption process, water molecules are likely to donate electrons to the surface. As free orbitals of the surface are saturated, the ability of the surface to adsorb H_2O and NH_3 decreases.

3.3.2. Atom in molecular (AIM) analysis. Bader charge is calculated to quantify the electronic changes at Lewis acid sites associated with adsorption of water, as summarized in Table 2. The adsorption site corresponding to the latest adsorbed water molecule is analyzed. The hydrogens in water molecules tend to interact with terminal O(1) atoms from neighboring active sites. The Bader charge of both terminal O(1) sites were analyzed, and the average atomic charge value was calculated.

In the water adsorption process for 1 to 4 molecules, the electronegativity of both bridging and terminal oxygen atoms at the adsorption sites increases. Specifically, the addition of the second water molecule markedly enhances the electronegativity of terminal oxygen atoms. Yet, as water coverage expands, terminal oxygen's electronegativity plateaus, while the bridging oxygen atoms continue to become more electronegative. In both the fifth and sixth models, the water molecules were absorbed on other exposed titanium atoms, resulting in an increase in the electronegativity of the terminal oxygen atoms at the V_2O_5/TiO_2 interface. Meanwhile, the electronegativity of the bridging oxygen atoms remained stable. In configurations 9 to 12 (sub-9-H_2O to sub-12-H_2O), water molecules bind to the vanadium species, with one hydrogen of each molecule attracted to bridging oxygen and the other to terminal oxygen, affecting the electronegativity of bridging oxygen atoms. Combining these findings with thermodynamic analysis, the observed decrease in electronegativity indicates that the surface's adsorption capacity has been exceeded. The capacity to accept electrons from water molecules is crucial in this adsorption process.

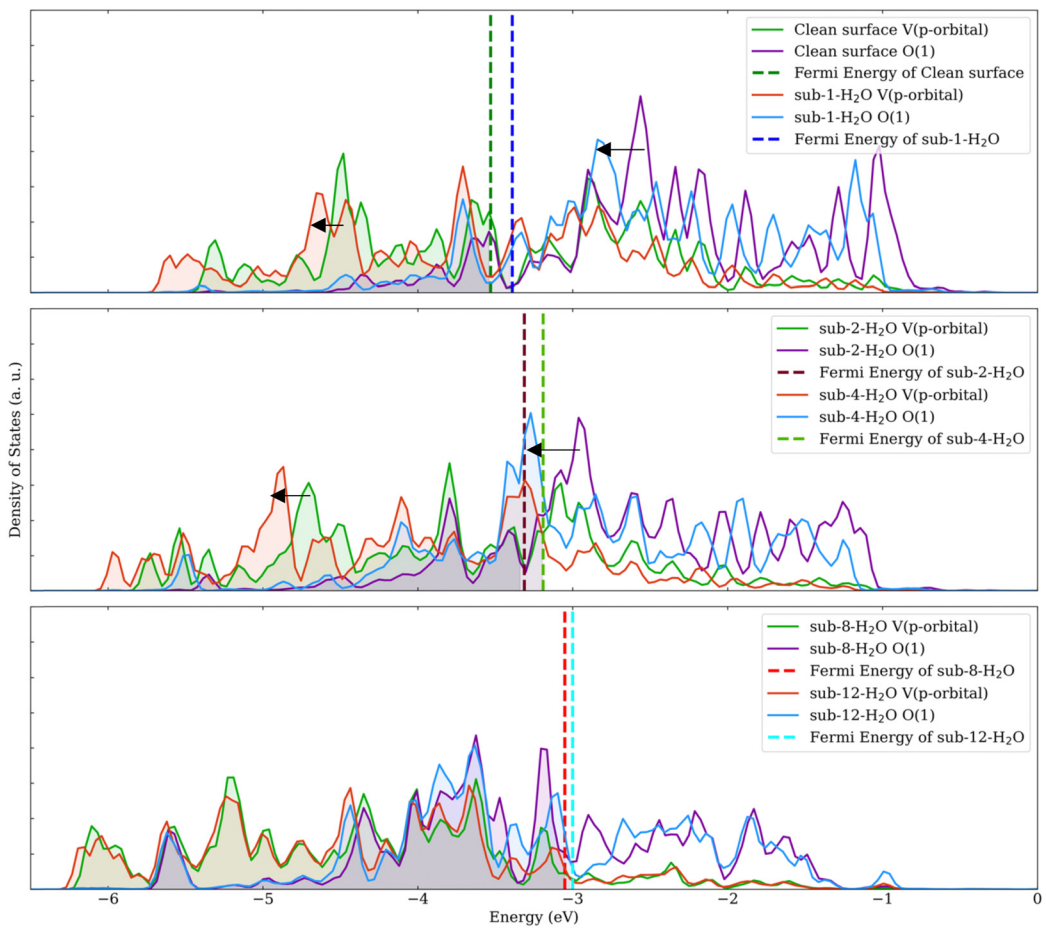

Fig. 4 Projected density of states of models with different water coverage levels. Black arrows indicate the shift of peaks.

Table 2 Summary of the atomic charge of oxygen atoms of the corresponding adsorption site

Surface atom	O(1)–H	O(1)–H	Avg O(1)–H	O (bridge)
sub-1-H_2O	−0.70	−0.66	−0.68	−0.86
sub-2-H_2O	−0.76	−0.99	−0.87	−0.88
sub-3-H_2O	−0.87	−0.87	−0.87	−0.91
sub-4-H_2O	−0.8	−0.93	−0.87	−1.03
sub-5-H_2O	−0.78	−0.72	−0.75	−1.04
sub-6-H_2O	−0.79	−0.82	−0.81	−1.03
sub-7-H_2O	−0.83	−0.79	−0.81	−1.01
sub-8-H_2O	−0.71	−0.97	−0.84	−1.01
sub-9-H_2O	−0.89	−0.75	−0.82	−1.08
sub-10-H_2O	−0.72	−0.88	−0.80	−1.10
sub-11-H_2O	−0.85	−0.79	−0.82	−1.13
sub-12-H_2O	−0.73	−0.92	−0.83	−1.09

3.3.3. Electron density difference. Another approach toward understanding the changes in electronic structure induced by the adsorbed water molecule is through electron density difference. The electron density difference is calculated by subtracting the electron density of H_2O and the clean substrate from the adsorbed model. We utilized the sub-1-H_2O model to examine the electronic alterations with the exposed titanium atom during the adsorption process. Fig. 5(a) depicts the isosurfaces of the calculated electron density difference; here, yellow denotes an increase in electron density, while cyan indicates a decrease. Notably, the hydrogen atom in the water molecule is drawn towards two terminal oxygens from V_2O_5, leading to a shift of electrons from the oxygen atom in water and the exposed titanium atom towards the vanadium species. This increase in electron density results in a reduced acidity at the Lewis acid sites. Fig. 5(b) illustrates the local integral curve, further confirming electrons are drawn towards the Lewis acid sites, thus decreasing the acidity of the surface. Additionally, the enhanced electron density suggests the formation of Brønsted acid sites, consistent with experimental observations reported by Inomata *et al.*[11]

A significant difference in electronic density around the exposed titanium atom is observed. To better understand the contribution of the titanium support, a monolayer model with an adsorbed water molecule was employed. The effect of the exposed titanium atom is less evident in this model given the separation. Hydrogen atoms in the water molecule are attracted to two oxygen atoms: one bridging and one terminal. The electronic density change is confined to the monolayer V_2O_5 region. Although a decrease in electron density is still evident around the water molecule, it is less pronounced in the absence of an exposed titanium atom. This observation aligns with the lower adsorption energy of water when positioned vertically above V_2O_5 sites. These observations suggest that exposed titanium atoms play a major role in both enhancing water adsorption and weakening the acidity of Lewis acid sites when water is present.

The impact of adsorbed water molecules on the electronic structure was investigated. The PDOS analysis suggests notable increases of Fermi level are significant, suggesting the adsorbed H_2O molecules saturated free orbitals of the V_2O_5/TiO_2 surface. The AIM analysis found increases in electronegativity of the Lewis acid sites neighboring adsorbed H_2O, indicating the acidity becomes weakened as the level of water coverage rises. The electron density difference revealed the role of TiO_2 support during the adsorption of water. Exposed titanium atoms increase the electronegativity at Lewis acid sites, leading to a reduction in the acidity of Lewis sites in the presence of water.

3.4. *Ab initio* thermal dynamic analysis

3.4.1. Gibbs free energy as a function of water coverage and temperature. The adsorption energy offers insights into the adsorption configurations; however, it should be noted the DFT calculations are limited to the ground states. To acquire a deeper understanding of the thermodynamic behavior at temperatures relevant to industrial applications of the V_2O_5/TiO_2 deNO_x catalysts, the Gibbs free energy for models with varying water coverage was further examined.

This study employed a methodology similar to those described by Galimberti *et al.*[55] and Wilcox *et al.*[23] The vibrational contribution of the substrate is neglected, as Rogal *et al.*[54] found that the impact of temperature on the vibrational contribution of metal oxide surfaces is minimal and fairly consistent, while the vibrational contribution of the gas species cannot be ignored.

The selective vibrational analysis was performed to obtain the vibrational contribution of the gas molecules. Fig. 6(a) illustrates the vibrational contributions for different numbers of adsorbed H_2O molecules. As the temperature increases, there is an overall decrease in vibrational contribution. While more water molecules inhabit the surface, some low frequencies are emerging due to interaction between the surface and water molecules. In the context of the harmonic approximation, frequencies below 50 cm^{-1} are treated as 50 cm^{-1}. The contribution of vibrational energy is a proxy to represent the effect of dissociation of water molecules for low water coverage models.

Gibbs free energy of adsorption is calculated based on eqn (2). At temperatures below 200 K, even the models with extremely high coverage of water are thermodynamically favorable. However, as temperatures rise, these systems, particularly those with higher water loadings, become less thermodynamically stable. The system fully saturated with water (sub-12-H_2O) becomes unfavorable below 200 K, indicating a water adsorption threshold. Water molecules are likely to be adsorbed at the interface of V_2O_5 and TiO_2. Furthermore, the high Gibbs energy barrier renders this system impractical in real-world temperatures. In the sub-8-H_2O model, titanium atoms and terminal oxygens of V_2O_5 are fully covered. This configuration remains thermodynamically favorable up to 280 K. Configurations with 4 and 2 adsorbed water molecules are thermodynamically favorable within the range of real-world working temperatures for SCR catalysts. Specifically, models with 4 water molecules remain favorable until 390 K, and the model with 2 water molecules until 440 K. The configuration with a single water molecule adsorbed to an undercoordinated titanium atom is the most thermodynamically stable and remains favorable up

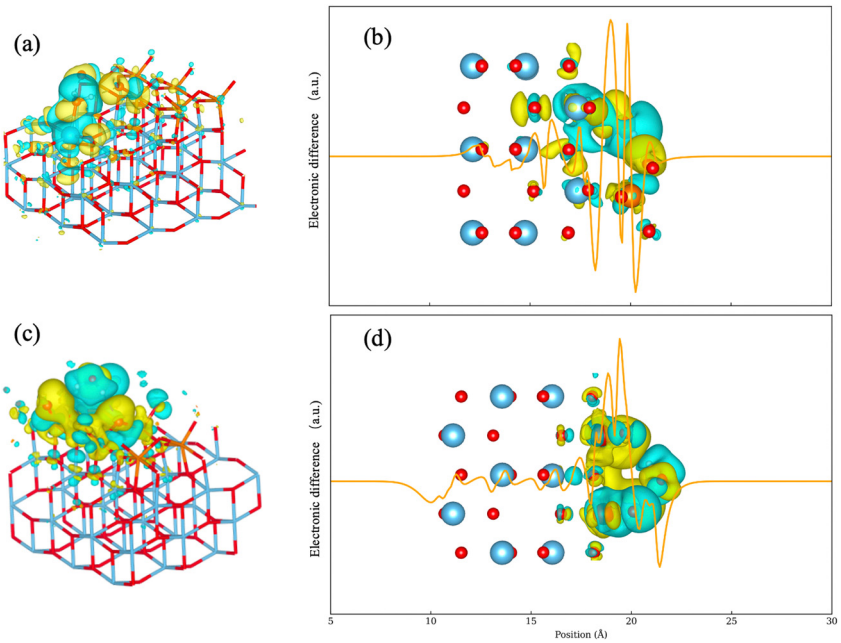

Fig. 5 Isosurfaces of electron density difference and local integral curve; the electron density increases in the yellow regions, and decreases in the cyan regions. (a) Side view of model sub-1-H_2O with isosurfaces of electron density difference; (b) local integral curve along the *Z* axis of the model sub-1-H_2O with isosurfaces of electron density difference; (c) side view of model mono-1-H_2O with isosurfaces of electron density difference; (d) local integral curve along the *Z* axis of model mono-1-H_2O with isosurfaces of electron density difference.

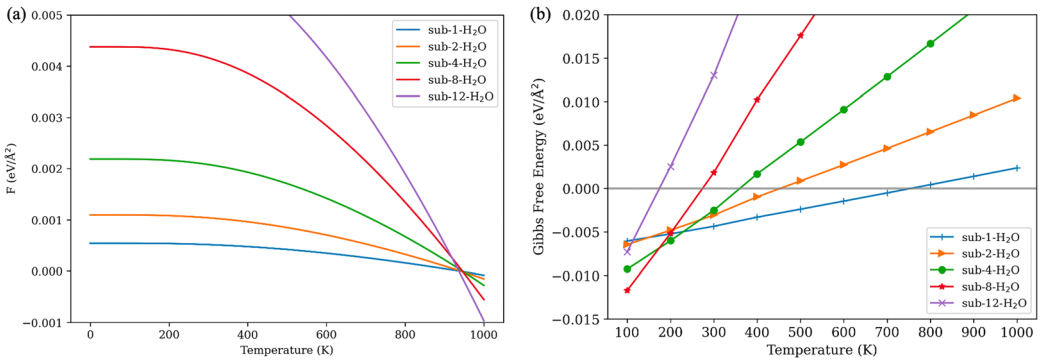

Fig. 6 (a) Vibrational contributions for different numbers of adsorbed H_2O molecules; (b) Gibbs free energy of adsorption for different numbers of adsorbed H_2O molecules.

to 750 K, suggesting chemical adsorption and potential dissociation of a water molecule as observed in the molecular dynamic simulation.

The outcomes of thermodynamic calculations indicate that water-induced deactivation of the catalyst can be reversed by increasing the temperature of the gas stream to 400 K and above, as observations from existing experimental studies found.[11,13,69,70] However, achieving complete desorption of water from the surface at application temperatures is nearly impossible, as suggested by the Gibbs free energy of adsorption yielded from the model sub-1-H_2O. Prolonged exposure to a humid gas stream may lead to surface reconstruction of V_2O_5/TiO_2 catalysts, potentially causing irreversible deactivation.[70–72]

3.4.2. NH_3 adsorption at V_2O_5/TiO_2 with different levels of water coverage. In the SCR reaction mechanism, NH_3 adsorption on the catalyst surface is a critical step, regardless of the surface configuration and the reaction pathway. Additionally, adsorbed NH_3 species participate in SCR reactions. Consequently, it is unlikely for the SCR surface to serve as a storage medium for NH_3. This study aims to investigate NH_3 adsorption in relation to varying levels of water adsorption. As this study intends to reveal its adsorption with correlation to different levels of water adsorption, we limit the number of NH_3 to one. There is long argument about the nature of the active sites, Marberger *et al.*[34] observed that the Lewis acid site is the primary site for the SCR reaction, while Brønsted acid sites served as a storage of NH_3, and this theory is also

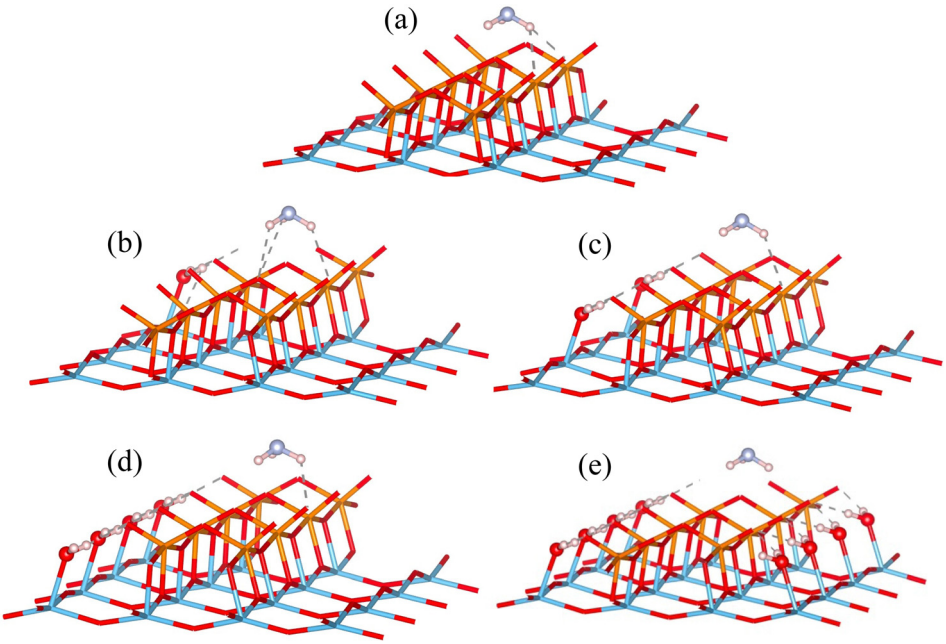

Fig. 7 NH_3 adsorption configurations at different water adsorbed levels. (a) to (e): 0, 1, 2, 4, and 8 H_2O molecule(s) adsorbed. Red are oxygen atoms, blue are titanium atoms, orange are vanadium atoms, light pink are hydrogen atoms, and sky blue are nitrogen atoms; the 2 bottom layers of TiO_2 support are hidden for clarity.

supported by others.[72–75] To represent the reactivity of SCR catalysts more accurately, the adsorption of NH_3 is modeled with a similar approach as H_2O.

The adsorption configuration is determined by surface scans of adsorption energy over the Lewis acid sites, for each configuration with different level water coverage. Fig. 7 displays the resulting adsorption configurations. The position of adsorbed NH_3 molecule is only slightly influenced by the configuration of water molecules. As the coverage of water increases, the adsorption energy of NH_3 decreases, accompanied by an increase in the distance between the NH_3 molecule and the Lewis acid sites.

The Gibbs free energy of adsorption of NH_3 presents a complex picture. On a clean surface (sub-NH_3), the Gibbs free energy of adsorption of NH_3 is smaller than every co-sorption model with water adsorbed on the surface at 100 K, as shown in Fig. 8. However, 100 K is not a meaningful temperature for the NO_x removal reactions. The adsorption of NH_3 on the clean V_2O_5/TiO_2 surface keeps being thermodynamically favorable until almost 500 K, truing less favorable slowly. Models with low water loading, particularly those with low water coverage (namely sub-1-H_2O–NH_3 and sub-2-H_2O–NH_3), demonstrate high stability as well. The temperature at which the Gibbs free energy of adsorption for the model sub-2-H_2O–NH_3 reaches zero (460 K) is slightly higher than that for the model without NH_3 loading (sub-2-H_2O, 430 K). Models with a higher degree of water coverage are less thermodynamically stable.

The models featuring 4 and 8 adsorbed water molecules, which cover half and the entirety of the exposed titanium area respectively (sub-4-H_2O–NH_3 and sub-8-H_2O–NH_3), is very thermodynamically unfavorable. The sub-4-H_2O–NH_3 model becomes thermodynamically unfavorable at 310 K, while the

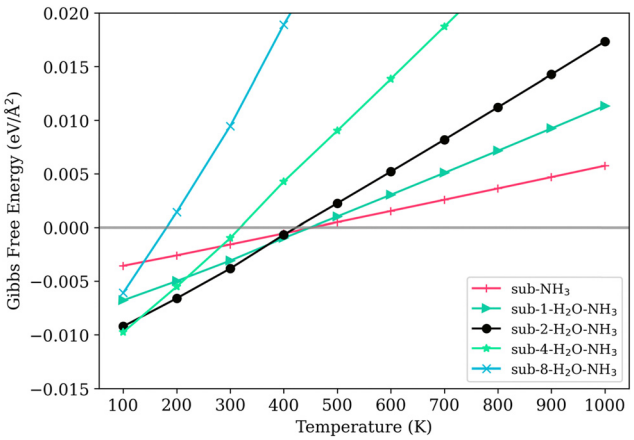

Fig. 8 The Gibbs free energy of adsorption of NH_3 on the surface with different levels of water adsorption.

sub-8-H_2O–NH_3 model becomes unfavorable at a much lower temperature of 80 K. In contrast, their corresponding models without NH_3, sub-4-H_2O and sub-8-H_2O, remain stable even when the temperature is raised to 400 K and 270 K, respectively. This distinct decrease can indicate that NH_3 is less likely to be absorbed on the Lewis sites with a water coverage level higher than 35%, thus increases the energy barrier of the catalytic reaction, resulting in lower catalytic activity.

To further understand the effect of water coverage levels on reactivity, a rate constant in an Arrhenius form was proposed: R^{Ads}, as described in eqn (4). The purpose of this constant is to establish a link between the microscale model and the

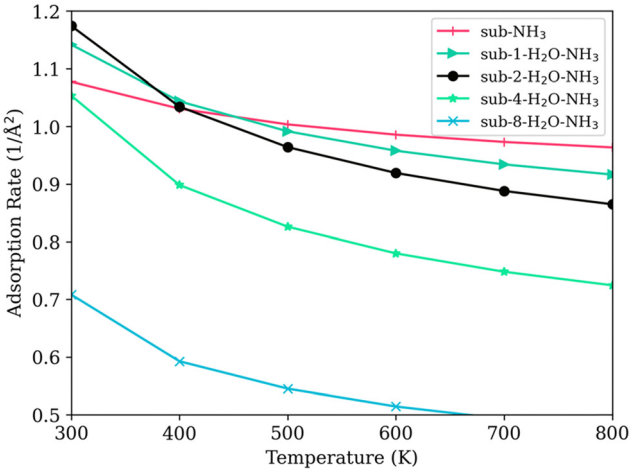

Fig. 9 Temperature and the adsorption rate of NH_3 on SCR surfaces with varying water coverage levels.

macroscale reaction dynamics. This rate constant can be effectively utilized for comparative analysis between different models that employ identical computational approaches, and it can also be used to explain changes in reactivity observed experimentally. We acknowledge that this constant has limited applicability for quantitative analysis of macroscale reaction rates.

As shown in Fig. 9, the adsorption rate for the model with no water (sub-NH_3) decreases slowly as the temperature increases. For models with low levels of water coverage ($<15\%$) (model sub-1-H_2O–NH_3 and sub-2-H_2O–NH_3), the presence of water initially increased the adsorption rate of NH_3. The increase of adsorption rate can indicate an increase in activity at low temperatures under a low humid gas stream, aligning with the observations of Inomata *et al.*.[11,13] Interestingly, this enhanced adsorption rate contradicts the predictions made by the PDOS calculations. This discrepancy could be attributed to the potential dissociation of water molecules, an effect that is not directly reflected in PDOS but is captured in the zero-point vibrational energy calculations.

As the number of adsorbed water molecules increases to four and eight, covering half and then the entire titanium surface (sub-4-H_2O–NH_3 and sub-8-H_2O–NH_3), the adsorption rate of NH_3 decreases markedly at temperatures below 400 K. These decreases indicate a strong competitive adsorption effect: water molecules hinder the ability of Lewis acid sites to adsorb NH_3.

3.4.3. Reversing water-induced deactivation. Existing experimental findings demonstrate that water-induced deactivation of catalysts is reversible.[69,71,72] Typically, catalyst activity can be reinstated at temperatures above 400 K. This recovery in activity is likely due to the desorption of water molecules from the surface with rising temperatures. Systems with extensive water coverage prove to be thermodynamically unfavorable at elevated temperatures, as depicted in Fig. 6(b) and Fig. 8. For catalysts deactivated by water, elevating the temperature makes the system thermodynamically unfavorable, thereby facilitating water desorption. Consequently, the NH_3 adsorption rate can be restored to levels observed with no water or a lower level of water adsorption, potentially reviving the catalytic activity.

Ab initio thermodynamic analysis of models with varying water coverages indicates that water-induced deactivation of the catalyst is reversible by increasing the gas stream temperature to 400 K or above, a well-established procedure in the industry. However, complete water desorption at application temperatures is difficult, and long-term exposure to humid gas streams might lead to irreversible deactivation. Interestingly, at low water coverage ($\leq 35\%$), co-adsorption of NH_3–H_2O is more favorable than NH_3 adsorption on a clean V_2O_5/TiO_2 surface, thermodynamically. Low levels of water coverage ($\leq 35\%$) can even enhance the NH_3 adsorption rate at temperatures lower than 400 K.

3.5. Pathways to enhance water resistance

These findings suggest multiple pathways to mitigate water-induced deactivation. One approach is to use a support material with weaker interactions with water, improving water resistance while minimally affecting Lewis acid sites. Introducing species like tungsten oxides to the V_2O_5/TiO_2 surface could shield exposed titanium atoms, limiting electronic changes during water adsorption. Alternatively, replacing vanadium with a different active element could increase the availability of Lewis acid sites, enhancing resistance to water. Finally, coating the TiO_2 area with a highly non-polar species could significantly boost the acidity of Lewis acid sites and potentially create hydrophobicity.

4. Conclusions

This work presented and validated stable models of the V_2O_5/TiO_2 surface. The adsorption of water is enhanced by exposed titanium atoms, particularly at the V_2O_5/TiO_2 interface. While low water coverage leads to dissociative adsorption, the TiO_2 support maintains its stability at higher coverage levels. Water adsorption significantly alters the catalyst's electronic structure, including an increase in the Fermi level that suggests saturation of surface free orbitals. Additionally, water weakens the acidity of Lewis acid sites as coverage increases. Exposed titanium atoms play a key role in reducing Lewis acidity *via* adsorbed water. *Ab initio* thermodynamic analysis established the reversibility of water-induced catalyst deactivation at temperatures above 400 K, consistent with established industrial practices. Complete water desorption is difficult at typical operating temperatures. Low water coverage ($\leq 35\%$) demonstrates a thermodynamically favorable co-adsorption of NH_3–H_2O compared to NH_3 alone on a clean V_2O_5/TiO_2 surface. However, prolonged exposure to humid conditions poses a risk of irreversible deactivation, as the TiO_2 surface could be dissociated.

Our findings suggest multiple pathways to mitigate water-induced deactivation in V_2O_5/TiO_2 catalysts. Strategies include using a support material less prone to water interaction, shielding exposed titanium atoms with additives, employing an alternative active element to vanadium, or coating the TiO_2

area with a highly non-polar species to enhance acidity and potentially achieve hydrophobicity.

Data availability

Data for this paper, including geometry data for gas species and crystallographic data for V_2O_5/TiO_2, are available at **https://github.com/ducksalted/v2o5tio2**.

Conflicts of interest

The authors declare no competing interests.

Acknowledgements

This work was sponsored by the National Natural Science Foundation of China (Grants No. 52204414), the National Energy-Saving and Low-Carbon Materials Production and Application Demonstration Platform Program (TC220H06N), the National Key R&D Program of China (Grants No. 2021YFC1910504), and the Fundamental Research Funds for the Central Universities (Grants No. FRF-TP-20-097A1Z).

References

1 J. S. Gaffney, G. E. Streit, J. H. Hall and W. D. Spall, Beyond acid rain. Do soluble oxidants and organic toxinsinteract with SO2 and NO_x to increase ecosystem effects?, *Environ. Sci. Technol.*, 1987, **21**, 519–524.

2 H. He, Y. Wang, Q. Ma, J. Ma, B. Chu, D. Ji, G. Tang, C. Liu, H. Zhang and J. Hao, Mineral dust and NO_x promote the conversion of SO_2 to sulfate in heavy pollution days, *Sci. Rep.*, 2014, **4**, 4172.

3 G. B. Marks, W. Ezz, N. Aust, B. G. Toelle, W. Xuan, E. Belousova, C. Cosgrove, B. Jalaludin and W. T. Smith, Respiratory Health Effects of Exposure to Low-NO_x Unflued Gas Heaters in the Classroom: A Double-Blind, Cluster-Randomized, Crossover Study, *Environ. Health Perspect.*, 2010, **118**, 1476–1482.

4 J. L. Laughner and R. C. Cohen, Direct observation of changing NO $_x$ lifetime in North American cities, *Science*, 1979, **366**, 723–727.

5 J. K. Lai and I. E. Wachs, A Perspective on the Selective Catalytic Reduction (SCR) of NO with NH3 by Supported V2O5–WO3/TiO2 Catalysts, *ACS Catal.*, 2018, **8**, 6537–6551.

6 L. J. Muzio, G. C. Quartucy and J. E. Cichanowicz, Overview and status of post-combustion NO_x control: SNCR, SCR and hybrid technologies, *Int J. Environ. Pollut.*, 2002, **17**, 4–30.

7 S. Djerad, M. Crocoll, S. Kureti, L. Tifouti and W. Weisweiler, Effect of oxygen concentration on the NO_x reduction with ammonia over V2O5–WO3/TiO2 catalyst, *Catal. Today*, 2006, **113**, 208–214.

8 Z. Ma, X. Wu, Y. Feng, Z. Si, D. Weng and L. Shi, Low-temperature SCR activity and SO2 deactivation mechanism of Ce-modified V2O5–WO3/TiO2 catalyst, *Prog. Nat. Sci.: Mater. Int.*, 2015, **25**, 342–352.

9 B. Ye, B. Jeong, M. Lee, T. H. Kim, S.-S. Park, J. Jung, S. Lee and H.-D. Kim, Recent trends in vanadium-based SCR catalysts for NO_x reduction in industrial applications: stationary sources, *Nano Convergence*, 2022, **9**, 51.

10 B.-L. Zhang, L.-F. Deng, B. Liu, C.-Y. Luo, M. Liebau, S.-G. Zhang and R. Gläser, Synergistic effect of cobalt and niobium in Co3-Nb-Ox on performance of selective catalytic reduction of NO with NH3, *Rare Met.*, 2022, **41**, 166–178.

11 Y. Inomata, H. Kubota, S. Hata, E. Kiyonaga, K. Morita, K. Yoshida, N. Sakaguchi, T. Toyao, K. Shimizu, S. Ishikawa, W. Ueda, M. Haruta and T. Murayama, Bulk tungsten-substituted vanadium oxide for low-temperature NO_x removal in the presence of water, *Nat. Commun.*, 2021, **12**, 557.

12 Z. Lian, Y. Li, W. Shan and H. He, Recent Progress on Improving Low-Temperature Activity of Vanadia-Based Catalysts for the Selective Catalytic Reduction of NO_x with Ammonia, *Catalysts*, 2020, **10**, 1421.

13 Y. Inomata, S. Hata, M. Mino, E. Kiyonaga, K. Morita, K. Hikino, K. Yoshida, H. Kubota, T. Toyao, K. Shimizu, M. Haruta and T. Murayama, Bulk Vanadium Oxide versus Conventional V_2O_5/TiO_2: NH_3 –SCR Catalysts Working at a Low Temperature Below 150 °C, *ACS Catal.*, 2019, **9**, 9327–9331.

14 M. Qing, S. Su, K. Qian, L. Liu, Z. Yin, S. Hu, Y. Wang and J. Xiang, Insight into the catalytic performance and NH3 adsorption under high concentration of CO2 and/or H2O conditions on selective catalytic reduction of NO by NH3 over V2O5-WO3/TiO2 catalyst, *Fuel*, 2021, **286**, 119478.

15 Y. Inomata, H. Kubota, S. Hata, E. Kiyonaga, K. Morita, K. Yoshida, N. Sakaguchi, T. Toyao, K. Shimizu, S. Ishikawa, W. Ueda, M. Haruta and T. Murayama, Bulk tungsten-substituted vanadium oxide for low-temperature NO_x removal in the presence of water, *Nat. Commun.*, 2021, **12**, 557.

16 A. Vejux and P. Courtine, Interfacial reactions between V2O5 and TiO2 (anatase): Role of the structural properties, *J. Solid State Chem.*, 1978, **23**, 93–103.

17 M. Inomata, K. Mori, A. Miyamoto, T. Ui and Y. Murakami, Structures of supported vanadium oxide catalysts. 1. Vanadium(V) oxide/titanium dioxide (anatase), vanadium(V) oxide/titanium dioxide (rutile), and vanadium(V) oxide/titanium dioxide (mixture of anatase with rutile), *J. Phys. Chem.*, 1983, **87**, 754–761.

18 R. Saleh, The interaction of V2O5 with Ti02(anatase): Catalyst evolution with calcination temperature and O-xylene oxidation, *J. Catal.*, 1986, **98**, 102–114.

19 R. Kozlowski, R. F. Pettifer and J. M. Thomas, X-ray absorption fine structure investigation of vanadium(V) oxide-titanium(IV) oxide catalysts. 2. The vanadium oxide active phase, *J. Phys. Chem.*, 1983, **87**, 5176–5181.

20 Y. Wu, X. Zhou, T. Mi, M. Xu, L. Zhao and Q. Lu, Theoretical insight into the interaction mechanism between V2O5/TiO2 (0 0 1) surface and arsenic oxides in flue gas, *Appl. Surf. Sci.*, 2021, **535**, 147752.

21 G. C. Bond, Preparation and properties of vanadia/titania monolayer catalysts, *Appl. Catal., A*, 1997, **157**, 91–103.
22 M. Calatayud, B. Mguig and C. Minot, A periodic model for the V2O5–TiO2 (anatase) catalyst. Stability of dimeric species, *Surf. Sci.*, 2003, **526**, 297–308.
23 A. Suarez Negreira and J. Wilcox, DFT Study of Hg Oxidation across Vanadia-Titania SCR Catalyst under Flue Gas Conditions, *J. Phys. Chem. C*, 2013, **117**, 1761–1772.
24 Z. Lian, Y. Li, W. Shan and H. He, Recent Progress on Improving Low-Temperature Activity of Vanadia-Based Catalysts for the Selective Catalytic Reduction of NO_x with Ammonia, *Catalysts*, 2020, **10**, 1421.
25 A. Marberger, M. Elsener, D. Ferri and O. Kröcher, VOx Surface Coverage Optimization of V2O5/WO3-TiO2 SCR Catalysts by Variation of the V Loading and by Aging, *Catalysts*, 2015, **5**, 1704–1720.
26 X. Lang, T. Wang, Z. Wang, L. Li, C. Yao and K. Cai, Reasonable design of a V2O5-x/TiO2 active interface structure with high polysulfide adsorption energy for advanced lithium-sulfur batteries, *Electrochim. Acta*, 2022, **403**, 139723.
27 T. Mi, Y. Wu, X. Zhou, W. Li, L. Zhao, J. Liu and Q. Lu, Catalytic oxidation of CO over V2O5/TiO2 and V2O5-WO3/TiO2 catalysts: A DFT study, *Fuel Process. Technol.*, 2021, **213**, 106678.
28 L. Zheng, M. Casapu, M. Stehle, O. Deutschmann and J.-D. Grunwaldt, Selective catalytic reduction of NOx with ammonia and hydrocarbon oxidation over V_2O_5-MoO_3/TiO_2 and V_2O_5-WO_3/TiO_2 SCR catalysts, *Top. Catal.*, 2018, **62**, 129–139.
29 J. P. Chen and R. T. Yang, Role of WO3 in mixed V2O5-WO3/TiO2catalysts for selective catalytic reduction of nitric oxide with ammonia, *Appl. Catal., A*, 1992, **80**, 135–148.
30 J. K. Lai and I. E. Wachs, A Perspective on the Selective Catalytic Reduction (SCR) of NO with NH3 by Supported V2O5-WO3/TiO2 Catalysts, *ACS Catal.*, 2018, **8**, 6537–6551.
31 W. H. Weinberg, Eley−Rideal Surface Chemistry: Direct Reactivity of Gas Phase Atomic Hydrogen with Adsorbed Species, *Acc. Chem. Res.*, 1996, **29**, 479–487.
32 K. V. Kumar, K. Porkodi and F. Rocha, Langmuir–Hinshelwood kinetics – A theoretical study, *Catal. Commun.*, 2008, **9**, 82–84.
33 B. Zhang, S. Zhang and B. Liu, Effect of oxygen vacancies on ceria catalyst for selective catalytic reduction of NO with NH3, *Appl. Surf. Sci.*, 2020, **529**, 147068.
34 A. Marberger, D. Ferri, M. Elsener and O. Kröcher, The Significance of Lewis Acid Sites for the Selective Catalytic Reduction of Nitric Oxide on Vanadium-Based Catalysts, *Angew. Chem., Int. Ed.*, 2016, **55**, 11989–11994.
35 T. D. Kühne, M. Iannuzzi and M. Del Ben, *et al.*, CP2K: An electronic structure and molecular dynamics software package - Quickstep: Efficient and accurate electronic structure calculations, *J. Chem. Phys.*, 2020, **152**(19), 194103.
36 J. P. Perdew, K. Burke and M. Ernzerhof, Generalized Gradient Approximation Made Simple, *Phys. Rev. Lett.*, 1996, **77**, 3865–3868.
37 Y. Zhang and W. Yang, Comment on ''Generalized Gradient Approximation Made Simple'', *Phys. Rev. Lett.*, 1998, **80**, 890.
38 D. Vilela Oliveira, J. Laun, M. F. Peintinger and T. Bredow, BSSE-correction scheme for consistent Gaussian basis sets of double- and triple-zeta valence with polarization quality for solid-state calculations, *J. Comput. Chem.*, 2019, **40**, 2364–2376.
39 S. Grimme, J. Antony, S. Ehrlich and H. Krieg, A consistent and accurate *ab initio* parametrization of density functional dispersion correction (DFT-D) for the 94 elements H-Pu, *J. Chem. Phys.*, 2010, **132**(15), 154104.
40 S. Grimme, S. Ehrlich and L. Goerigk, Effect of the damping function in dispersion corrected density functional theory, *J. Comput. Chem.*, 2011, **32**, 1456–1465.
41 A. S. Negreira and J. Wilcox, Role of WO3 in the Hg oxidation across the V2O 5-WO3-TiO2 SCR catalyst: A DFT study, *J. Phys. Chem. C*, 2013, **117**, 24397–24406.
42 J. Li, Y. Peng, H. Chang, X. Li, J. C. Crittenden and J. Hao, Chemical poison and regeneration of SCR catalysts for NO x removal from stationary sources, *Front. Environ. Sci. Eng.*, 2016, **10**, 413–427.
43 Y. Peng, J. Li, W. Si, J. Luo, Q. Dai, X. Luo, X. Liu and J. Hao, Insight into deactivation of commercial SCR catalyst by arsenic: An experiment and DFT study, *Environ. Sci. Technol.*, 2014, **48**, 13895–13900.
44 D. Wang, J. Luo, Q. Yang, J. Yan, K. Zhang, W. Zhang, Y. Peng, J. Li and J. Crittenden, Deactivation Mechanism of Multipoisons in Cement Furnace Flue Gas on Selective Catalytic Reduction Catalysts, *Environ. Sci. Technol.*, 2019, **53**, 6937–6944.
45 T. Lu and F. Chen, Multiwfn: A multifunctional wavefunction analyzer, *J. Comput. Chem.*, 2012, **33**, 580–592.
46 A. R. Hoy and P. R. Bunker, A precise solution of the rotation bending Schrödinger equation for a triatomic molecule with application to the water molecule, *J. Mol. Spectrosc.*, 1979, **74**, 1–8.
47 T. N. Olney, N. M. Cann, G. Cooper and C. E. Brion, Absolute scale determination for photoabsorption spectra and the calculation of molecular properties using dipole sum-rules, *Chem. Phys.*, 1997, **223**, 59–98.
48 K. Yang, J. Zheng, Y. Zhao and D. G. Truhlar, Tests of the RPBE, revPBE, τ-HCTHhyb, ωB97X-D, and MOHLYP density functional approximations and 29 others against representative databases for diverse bond energies and barrier heights in catalysis, *J. Chem. Phys.*, 2010, **132**(16), 164117.
49 K. Reuter, C. Stampf and M. Scheffler, *Handbook of Materials Modeling*, Springer Netherlands, Dordrecht, 2005, pp. 149–194.
50 J. Rogal, Stability, composition and function of palladium surfaces in oxidizing environments: A first-principles statistical mechanics approach, PhD thesis, Freie Universität, Berlin, 2006.
51 Y. Ikeda, B. Grabowski and F. Körmann, Ab initio phase stabilities and mechanical properties of multicomponent alloys: A comprehensive review for high entropy alloys and compositionally complex alloys, *Mater. Charact.*, 2019, **147**, 464–511.

52 B. Cheng, E. A. Engel, J. Behler, C. Dellago and M. Ceriotti, Ab initio thermodynamics of liquid and solid water, *Proc. Natl. Acad. Sci. U. S. A.*, 2019, **116**, 1110–1115.
53 Joseph W. Ochterski, Thermochemistry in Gaussian, **https://gaussian.com/wp-content/uploads/dl/thermo.pdf**, (accessed 13 January 2024).
54 J. Rogal and K. Reuter, Ab Initio Atomistic Thermodynamics for Surfaces: A Primer, *Experiment, Modeling and Simulation of Gas-Surface Interactions for Reactive Flows in Hypersonic Flights*, Educational Notes RTO-EN-AVT-142, Paper 2, RTO, Neuilly-sur-Seine, France, 2007, pp. 2-1–2-18, **http://www.rto.nato.int/abstracts.asp**.
55 D. R. Galimberti and J. Sauer, Chemically Accurate Vibrational Free Energies of Adsorption from Density Functional Theory Molecular Dynamics: Alkanes in Zeolites, *J. Chem. Theory Comput.*, 2021, **17**, 5849–5862.
56 M. Chase, *NIST-JANAF Thermochemical Tables*, American Institute of Physics, 4th edn, vol. 1, 1998.
57 I. E. Wachs and B. M. Weckhuysen, Structure and reactivity of surface vanadium oxide species on oxide supports, *Appl. Catal., A*, 1997, **157**, 67–90.
58 N. Y. Topsoe, J. A. Dumesic and H. Topsoe, Vanadia-Titania Catalysts for Selective Catalytic Reduction of Nitric-Oxide by Ammonia, *J. Catal.*, 1995, **151**, 241–252.
59 F. D. Hardcastle and I. E. Wachs, Determination of vanadium-oxygen bond distances and bond orders by Raman spectroscopy, *J. Phys. Chem.*, 1991, **95**, 5031–5041.
60 C. Wang, H. Li, X. Zhang, Y. Qiu, Q. Zhu, S. Xun, W. Yang, H. Li, Z. Chen and W. Zhu, Atomic-Layered α-V_2O_5 Nanosheets Obtained via Fast Gas-Driven Exfoliation for Superior Aerobic Oxidative Desulfurization, *Energy Fuels*, 2020, **34**, 2612–2616.
61 S. Soyer, A. Uzun, S. Senkan and I. Onal, A quantum chemical study of nitric oxide reduction by ammonia (SCR reaction) on V2O5 catalyst surface, *Catal. Today*, 2006, **118**, 268–278.
62 A. Vittadini and A. Selloni, Periodic Density Functional Theory Studies of Vanadia−Titania Catalysts: Structure and Stability of the Oxidized Monolayer, *J. Phys. Chem. B*, 2004, **108**, 7337–7343.
63 Y.-T. Gu, Y.-M. Gu, Q. Tao, X. Wang, Q. Zhu and J. Ma, Machine learning for prediction of CO_2/N_2/H_2O selective adsorption and separation in metal-zeolites, *J. Mater. Inf.*, 2023, **3**(3), 19.
64 Y. Wu, G. Gao and G. Wu, Self-assembled three-dimensional hierarchical porous V_2 O_5/graphene hybrid aerogels for supercapacitors with high energy density and long cycle life, *J. Mater. Chem. A*, 2015, **3**, 1828–1832.
65 R. J. G. Nuguid, D. Ferri, A. Marberger, M. Nachtegaal and O. Kröcher, Modulated Excitation Raman Spectroscopy of V_2O_5/TiO_2: Mechanistic Insights into the Selective Catalytic Reduction of NO with NH_3, *ACS Catal.*, 2019, **9**, 6814–6820.
66 I. E. Wachs, T. Kim and E. I. Ross, Catalysis science of the solid acidity of model supported tungsten oxide catalysts, *Catal. Today*, 2006, **116**, 162–168.
67 T. Ohsaka, F. Izumi and Y. Fujiki, Raman spectrum of anatase, TiO_2, *J. Raman Spectrosc.*, 1978, **7**, 321–324.
68 Th. Wolkenstein, Electron theory of catalysis on semiconductors, *Adv. Catal.*, 1960, **12**, 189–264.
69 J. A. Martín-Martín, M. Gallastegi-Villa, M. P. González-Marcos, A. Aranzabal and J. R. González-Velasco, Bimodal effect of water on V2O5/TiO2 catalysts with different vanadium species in the simultaneous NO reduction and 1,2-dichlorobenzene oxidation, *Chem. Eng. J.*, 2021, **417**, 129013.
70 S. Li, W. Huang, H. Xu, T. Chen, Y. Ke, Z. Qu and N. Yan, Alkali-induced deactivation mechanism of V2O5-WO3/TiO2 catalyst during selective catalytic reduction of NO by NH3 in aluminum hydrate calcining flue gas, *Appl. Catal., B*, 2020, **270**, 118872.
71 Q. Liang, J. Li, H. He, T. Yue and L. Tong, Effects of SO2 and H2O on low-temperature NO conversion over F-V2O5-WO3/TiO2 catalysts, *J. Environ. Sci.*, 2020, **90**, 253–261.
72 H. Chen, Y. Xia, R. Fang, H. Huang, Y. Gan, C. Liang, J. Zhang, W. Zhang and X. Liu, The effects of tungsten and hydrothermal aging in promoting NH3-SCR activity on V2O5/WO3-TiO2 catalysts, *Appl. Surf. Sci.*, 2018, **459**, 639–646.
73 G. Busca, G. Centi, L. Marchetti and F. Trifiro, Chemical and spectroscopic study of the nature of a vanadium oxide monolayer supported on a high-surface-area TiO $_2$ anatase, *Langmuir*, 1986, **2**, 568–577.
74 M. Zhu, J.-K. Lai, U. Tumuluri, Z. Wu and I. E. Wachs, Nature of Active Sites and Surface Intermediates during SCR of NO with NH $_3$ by Supported V_2O_5–WO_3/TiO_2 Catalysts, *J. Am. Chem. Soc.*, 2017, **139**, 15624–15627.
75 H. W. Siaka, C. Dujardin, A. Moissette and P. Granger, Revisiting the Impact of Tungsten on the Catalytic Properties of Ammonia-SCR V2O5-WO3/TiO2 Catalysts: Geometric vs. Electronic Effects, *Chemistry*, 2023, **5**, 294–313.